International Journal of Solids and Structures 51 (2014) 210–226

Contents lists available at ScienceDirect

International Journal of Solids and Structures

journal homepage: www.elsevier.com/locate/ijsolstr

Identification of the plastic behavior of aluminum plates under free air explosions using inverse methods and full-field measurements

K. Spranghers [a,*], I. Vasilakos [a,*], D. Lecompte [b], H. Sol [a], J. Vantomme [b]

[a] Department of Mechanics of Materials and Constructions, Vrije Universiteit Brussel (VUB), Pleinlaan 2, B-1050 Brussels, Belgium
[b] Department of Civil and Materials Engineering, Royal Military Academy (RMA), Av. De la Renaissance 30, B-1000 Brussels, Belgium

ARTICLE INFO

Article history:
Received 6 May 2013
Received in revised form 23 September 2013
Available online 8 October 2013

Keywords:
Inverse method
Free air explosions
Finite element model
Strain hardening
Plastic behavior of aluminum
Full-field measurements

ABSTRACT

This article describes an inverse method for the identification of the plastic behavior of aluminum plates subjected to sudden blast loads. The method uses full-field optical measurements taken during the first milliseconds of a free air explosion and the finite element method for the numerical prediction of the blast response. The identification is based on a damped least-squares solution according to the Levenberg–Marquardt formulation. Three different rate-dependent plasticity models are examined. First, a combined model based on linear strain hardening and the strain rate term of the Cowper–Symonds model, secondly, the Johnson–Cook model and finally, a combined model based on a bi-exponential relation for the strain hardening term and the strain rate term of the Cowper–Symonds model. A validation of the method and its sensitivity to measurement uncertainties is first provided according to virtual measurements generated with the finite element method. Next, the plastic behavior of aluminum is identified using measurements from real free air explosions obtained from a controlled detonation of C4. The results show that inverse methods can be successfully applied for the identification of the plastic behavior of metals subjected to blast waves. In addition, the material parameters identified with inverse methods enable the numerical prediction of the material's response with increased accuracy.

1. Introduction

Protecting structures against terrorism attacks or incidental explosions is an important challenge for engineers. A number of widely reported tragic incidents and industrial explosions have stimulated the development of new protection technologies over the last years. Engineers increasingly rely on finite element simulations as they provide a powerful tool to understand the complex structural mechanisms during blast load events. One of the major concerns using the finite element method to simulate the blast response is to find appropriate material models capable of predicting accurately the actual structural response during blast wave impact. An open question is whether material parameters extracted from standard testing can be used to accurately predict the response of a structure during a blast event.

For the case of metals, the quasi-static tensile test and the Split-Hopkinson Bar Test (SHBT) are two widely used standard experimental methods for the determination of the rate-independent and rate-dependent plastic behavior, respectively. However, these tests suffer from serious limitations, *e.g.* the use of rather simple geometries and the requirement for homogeneous deformation fields, which can introduce errors reducing the accuracy of the results. For the case of the Split-Hopkinson bar, although it allows the identification of the material's mechanical behavior under a wide range of strain rates, the results may not be representative for real scale applications as examined in this article. The SHB test uses very small specimens which are deformed at constant strain rate. Meanwhile, for free air explosions real scale specimens are used and subjected to non-constant and non-uniform strain rates during the period of deformation. Furthermore, the choice of using of a blast load test ensures loading conditions and deformation fields that are representative for the real life situation.

The plastic behavior identified from standard tests is merely an approximation that in many cases is insufficient or at least incomplete for the reliable simulation of complex deformation processes. To improve the quality of the identification action, some authors have proposed complementary tests using more complex test setups in combination with inverse methods (Ghouati and Gelin, 1998; Mahnken and Stein, 1996; Meuwissen, 1998). These tests can include complex loading conditions and complex geometries. The produced heterogeneity in the deformation fields can more efficiently approximate the real life situation. Consequently, the material models obtained from these tests will be more suitable for numerical simulations. A second advantage of complex tests in combination with inverse methods is that the total set of

* Corresponding authors. Tel.: +32 2 629 29 36 (K. Spranghers). Tel.: +32 2 626 29 83 (I. Vasilakos).
E-mail addresses: Ken.Spranghers@vub.ac.be (K. Spranghers), Ioannis.Vasilakos@vub.ac.be (I. Vasilakos).

0020-7683/$ - see front matter © 2013 Elsevier Ltd. All rights reserved.
http://dx.doi.org/10.1016/j.ijsolstr.2013.09.027

unknown material parameters can be simultaneously identified through a single experiment, while for standard tests a series of tests must be performed for full characterization. Finally, the use of full-field optical measurements allows homogenization and averaging of the identified parameters. As a result, the identified parameters are more representative for the total area of the material than those obtained from local measurement of strains with strain gages.

The identification of the material behavior based on complex tests has to fulfill two necessary requirements: first, a technique suitable for the measurement of the heterogeneous deformation fields and secondly, a methodology for material identification which correlates deformations with the transmitted internal forces since the analytical formulas used in standard tests are no longer valid. The first requirement is fulfilled with the use of full-field measurement techniques (Chu et al., 1985; Cordero et al., 2004; Cordero and Labbé, 2005; Nicoletto, 2002). In this article, the high-speed 3D digital image correlation (3D-DIC) technique is adopted to measure the displacement fields. The second requirement is fulfilled with the use of the so-called *inverse methods* combined with the finite element method (FEM).

The term *inverse method* refers to the methodology followed to solve the inverse problem. Inverting the principles of causality, the general inverse problem refers to the determination of the causes for a given effect. For the case of material identification, the given effect may be the material response whereas the causes are the material parameters which transform the acting load to a given and measurable response. More information about the fundamentals of inverse problems can be found in the excellent book of Tarantola (2004). The inverse problem for material identification was first introduced in 1937 by Förster (1937). Since then, inverse methods have been introduced in a wide range of disciplines to estimate a broad variety of material parameters (Jadhav et al., 1999; Hikawa et al., 2004; Ferin et al., 2004; Hoes et al., 2004; Trujillo and Busby, 1997; Panneton et al., 2003; De Visscher, 1995; Furukwaw and Yagawa, 1998; Yoshida et al., 2003; Hendriks et al., 2003; Kauer, 2006; Schiltges, 1999; Ardito et al., 2003).

Several authors have used inverse methods to identify the plastic behavior of metals for different types of loading. Flores et al. used an optimization algorithm to evaluate the efficiency of different hardening laws and yield loci in sheet forming (Flores et al., 2007). Grédiac and Pierron applied an inverse method based on virtual fields to identify the elasto-plastic constitutive parameters (Grédiac and Pierron, 2006). Yoshida et al. used an inverse approach to identify the elasto-plastic behavior of bimetallic sheets (Yoshida et al., 2003). Qu et al. applied parameter identification through inverse analysis for improved viscoelastic modeling based on recrystallization (Qu et al., 2005). Cooreman et al. presented a detailed study on the calculation of the sensitivity matrix for elasto-plastic identification (Cooreman et al., 2007). Coppieters et al. showed that inverse methods can be successfully used for the identification of the post-necking hardening behavior (Coppieters et al., 2011).

The aim of this article is to identify the strain hardening behavior of thin aluminum plates subjected to blast waves initiated from free air explosions. The objective of the authors is to present the use of inverse methods and full-field optical measurements for direct material identification of real scale structural components subjected to complex dynamic loading conditions for time periods less than 1 ms. To fulfill this purpose, the authors make use of the experimental observations of the responses of four identical aluminum plates exposed to controlled free air explosions. The identification is performed by using a damped least-squares solution based on the Levenberg–Marquardt formulation. The identification process for each of the four experiments is repeated for three different rate-dependent plasticity models. The first model is a combination of the simple linear hardening model with the strain rate term of the Cowper–Symonds model. The second model is the well-known Jonhson–Cook model and the third model is a combined model based on a bi-exponential relation for the strain hardening term and the strain rate term of the Cowper–Symonds model. Additional attention is paid to possible measurement uncertainties and the experimental conditions. Therefore, a study on the effect of measurement noise on the efficiency of the identification process through a series of virtual experiments is included. Moreover, the influence of the uncertainty on the explosive's location to the identified material behavior is highlighted. For this reason, the authors present a two-step identification strategy in which the position of the explosive is considered as an additional unknown parameter to the set of material parameters that the inverse method aims to identify. To evaluate the efficiency of the identification process, the obtained results are compared in terms of material response with those obtained by standard tests as well as with models provided by previous authors.

The article starts with a description of the experimental setup and the formulation of the numerical model. Next, a short introduction to inverse methods for material identification is provided. The article then presents the main part where the results of the identification process are discussed. First, the results based on the virtual experiments are provided where the effect of measurement noise is the main topic of discussion. Next, the results of the identification process based on real experimental data are presented. Finally, a series of conclusions extracted from the present work and some components of future work are provided.

2. Experimental setup

The authors of the present article recently published on the experimental methodology to perform and analyze a laboratory-scale free air blast test (Spranghers et al., 2012). The experiments are performed in the test bunker of the Laboratory of Analysis of Explosion Effects (LAEE) at the Royal Military Academy (RMA) in Brussels. The layout of the experimental setup is shown in Fig. 1(a). A thin aluminum plate ($400 \times 400 \times 3$ mm^3) with commercial code EN AW-1050A H24 (average elastic properties: $E = 62.5$ GPa and $\nu = 0.33$.) is fixed onto a steel frame with commercial code EN 10025-S235 and dimensions $1000 \times 1000 \times 15$ mm^3, using bolts and an aluminum clamping frame (see Fig. 1(c) and (e)). The clamping frame, with a thickness of 10 mm, is fabricated from aluminum with commercial code EN AW-7022. The steel frame has a square aperture, providing the specimen a blast impact area of 300×300 mm^2.

The explosive material is Composition C4 with an imperfect spherical shape (approx. diameter: 36.27 mm) and a mass of 40 g. An electronic detonator (type M75, 1 g TNT equivalent) is used to initiate the blast event. A detailed view of the explosive mass and the detonator is illustrated in Fig. 1(d). The explosive mass is positioned at a stand-off-distance of 250 mm from the center point of the plate in order to generate a spherical airburst wave.

To capture the dynamic response of the plate, the Digital Image Correlation (DIC) technique is used. For this reason, two Photron Fastcam SA5 high-speed digital cameras are mounted in a stereo configuration to record synchronized images during the free air blast event (see Fig. 1(b)). The high-speed cameras are positioned at a safety distance of 2500 mm from the plate in order to avoid damage and camera motion induced by the blast loading. In addition, the two cameras are rotated and focused in order to maximize the common field of view and the level of correlation. Since large out-of-plane displacements are expected, the aperture of both lenses is reduced (to increase the depth of view) and the aluminum

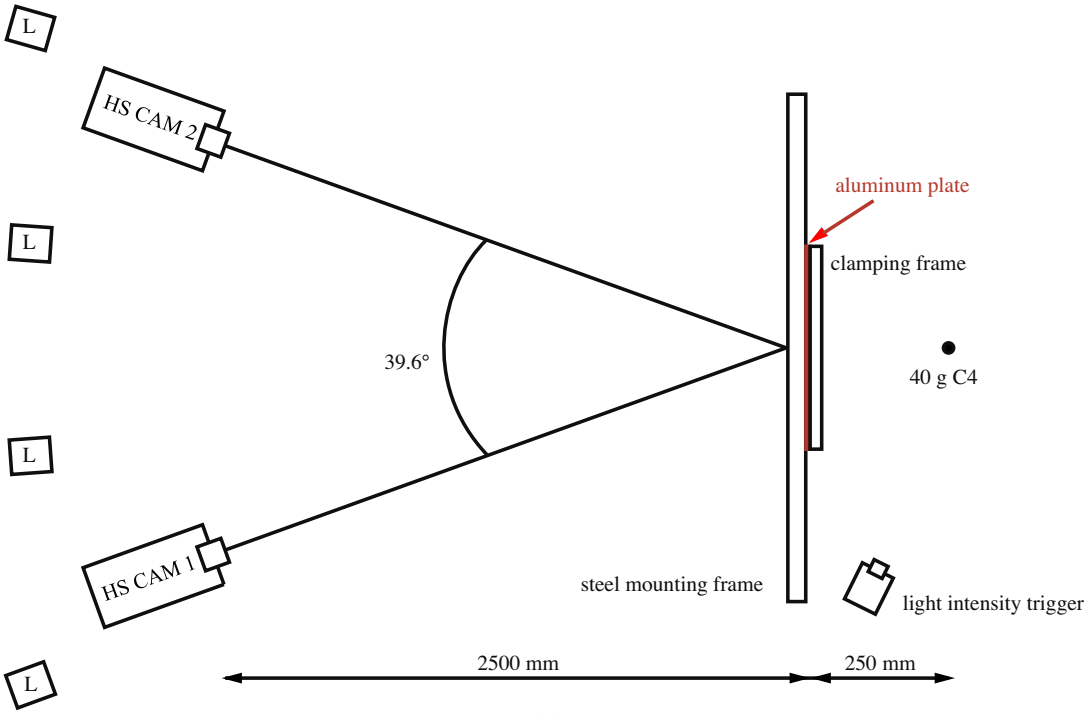

(a)

(b)

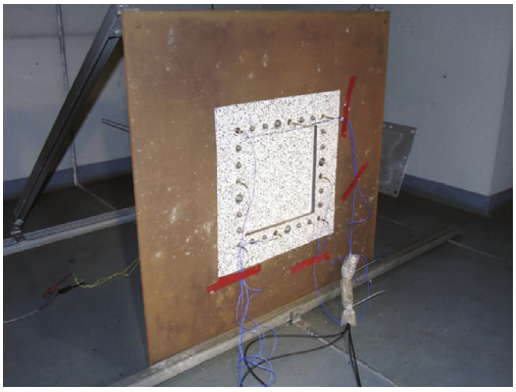

(c)

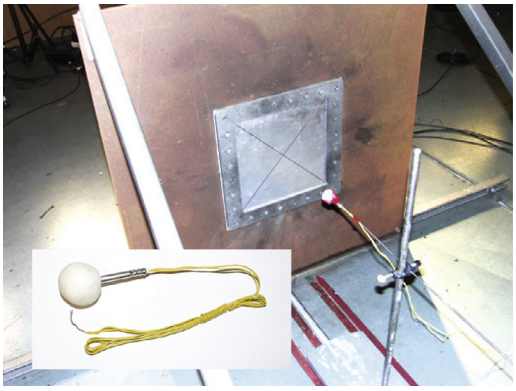

(d)

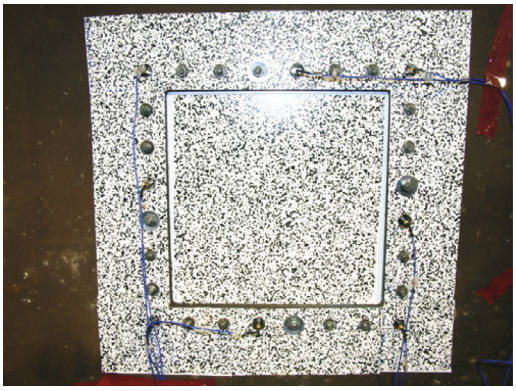

(e)

Fig. 1. The experimental setup: (a) setup's layout; (b) two high-speed digital cameras mounted in a stereo configuration and four light spots; (c) steel mounting plate and aluminum plate specimen; (d) spherical explosive and electronic detonator; (e) high contrast black and white speckle pattern.

sheet illumination (4 light spots with total electric power of 3300 Watt) is increased to compensate for the reduced aperture and maintain adequate contrast throughout the experiment. These settings ensure that the deformed sheet remains in focus. Finally, the high-speed stereo vision system is calibrated using a calibration panel and standard image correlation software as presented in Tiwari et al. (2007).

A light intensity trigger is placed near the detonation point and adjusted to ensure triggering by the bright light flash of the explosion, sending the starting signal to the high-speed cameras. As soon as the explosion initiates, synchronized stereo images at a frame rate of 25,000 fps and a shutter time of 25 μs are acquired. The surface of the aluminum plate is painted by application of a white background and a black speckle pattern to obtain high contrast images (see Fig. 1(e)). During the experiments the absolute (total) plate behavior is observed with a field of view of $\pm 500 \times 500$ mm^2 and an image size of 512×512 pixels. To obtain 3D full-field results (a) a reduced area of interest (aoi) of 200×200 pixels, (b) a 21×21 pixel subset, (c) a subset spacing of 3 pixels and (d) a strain filter size of 9 are selected. Finally, subset matching is performed using affine subset shape functions. Details about the working principle of the three-dimensional image correlation technique are available in Spranghers et al. (2012) and Sutton et al. (2009).

3. Numerical model

Different numerical techniques are available to analyze the dynamic response of structural components due to blast loading (Remennikov, 2003; Børvik et al., 2009). In this article the finite element method is used to numerically simulate the response of the aluminum plates under blast waves.

The authors of the present article recently published on the validation of the numerical simulation of the blast response of thin plates (Spranghers et al., 2012). Experimental data obtained from 3D high-speed digital image correlation was compared to data obtained from the finite element analysis. The influence of different features (element type, element size, integration scheme, *etc.*) on the accuracy of the numerical prediction was investigated. They concluded that a pure Lagrangian formulation, using a simplified blast load description based on ConWep (DATM, 1986), provides a fast and powerful tool to fulfill this assignment. The finite element model based on a shell formulation is capable of simulating the very fast material response and the use of an explicit integration scheme dramatically reduces the computational effort without significant loss of accuracy.

The following paragraphs provide a short description of the formulation of the finite element model and the modeling of the explosive loading. For more details the reader may refer to Spranghers et al. (2012).

3.1. Explosive loading

In this article the modeling of the explosive loading is performed using the empirical method developed by Kingery and Bulmash (1984) where air blast parameters from spherical airbursts and hemispherical surface bursts are predicted by empirical equations. These equations are widely accepted as engineering predictions to determine free field pressures and loads on structures. The Kingery–Bulmash equations have been automated in the computer program ConWep (DATM, 1986). Curve-fitting techniques are used to represent the data with high-order polynomial equations, assuming an exponential decay of the pressure with time. A functional form such as the Friedlander equation can model the typical pressure–time history in the vicinity of a free air explosion as follows:

$$P(t) = P_o + P_l\left(1 - \frac{t}{t_+}\right)e^{-a\frac{t}{t_+}} \tag{1}$$

where t_+ is the positive phase duration and parameter a the waveform number depending on the peak incident pressure, P_l (with P_o the reference ambient pressure). Values for the blast wave parameters t_+, P_l and a can be found in Kingery and Bulmash (1984), Baker et al. (1983) and Smith and Hetherington (1994).

Blast pressures in free air, or incident pressures, are seldom of interest as the focus of attention is on the interaction of these pressures with the structure and the subsequent response of the structure itself. When a blast wave encounters a structure the sudden decrease in velocity of the shock wave and particle velocities behind the shock gives rise to an increase in pressure, *i.e.* the reflected pressure. Due to the large compressibility of air, the reflected pressure is typically much more than doubled, $P_R = C_R P_I$ with $2 \leqslant C_R \leqslant 8$. The reflected pressure wave has a similar form as the incident pressure wave and can also be modeled by the Friedlander equation but with a different decay rate (waveform number). In the idealized case of ConWep there is no decay coefficient and the pressure wave is considered as a special triangular impulse because the structure is considered to be rigid and its surface infinite. ConWep is fully implemented in the finite element software Ls-Dyna by Randers-Pehrson and Bannister. It takes into account the decay coefficient and also updates the pressure–time history based on changes in the geometry (Randers-Pehrson and Bannister, 1997; LSTC, 2007). The objective of this algorithm is to produce an appropriate pressure history given an equivalent TNT explosive weight. The quantities to be determined by the algorithm are: the peak incident pressure P_I, the peak reflected pressure P_R, the time of arrival of the shock wave t_a, the positive phase duration t_+ and the exponential decay factors a, b for incident and reflected waves, respectively. The input values that need to be chosen are: the amount of explosive charge, the range R from the charge location to the centroid of the loaded surface and the angle $cos\theta$ between surface normal and range unit vector. The parameters that need to be defined by the user are the TNT-equivalent mass of the explosive and the position of the center of the explosion in space, which defines the stand-off-distance. For C4 a TNT-equivalence of 1.34 is used. This factor corresponds to the ratio between the mass specific energy of C4 and TNT, respectively.

Nominally identical detonations are known to regularly produce different loads on structures from test to test due to a series of non-controlled factors that affect the pressure profiles, such as the movement in space and time of the air particles which is unique for each detonation. In the authors' previous work (Spranghers et al., 2012; Spranghers et al., 2012) an experimental validation of the empirical blast load model is presented. It shows that the accuracy of the air burst model, in terms of sphericity and magnitude of reflected pressure, is significant and therefore the empirical model can be regarded as reliable. Furthermore, special attention needs to be paid to possible sources of errors that can cause asymmetry in the propagated pressure wave, such as the use of an electronic detonator, the shape of the explosive's mass and the location in space of the detonation point. In Section 6.3 a solution is presented to take into account the effects of asymmetric loading.

3.2. Shell model: parts and boundary conditions

The shell model of the clamped aluminum plate (see Fig. 1c) is shown in Fig. 2. It consists of 3 parts: an aluminum plate specimen (light gray), a steel mounting frame (brown) and an aluminum

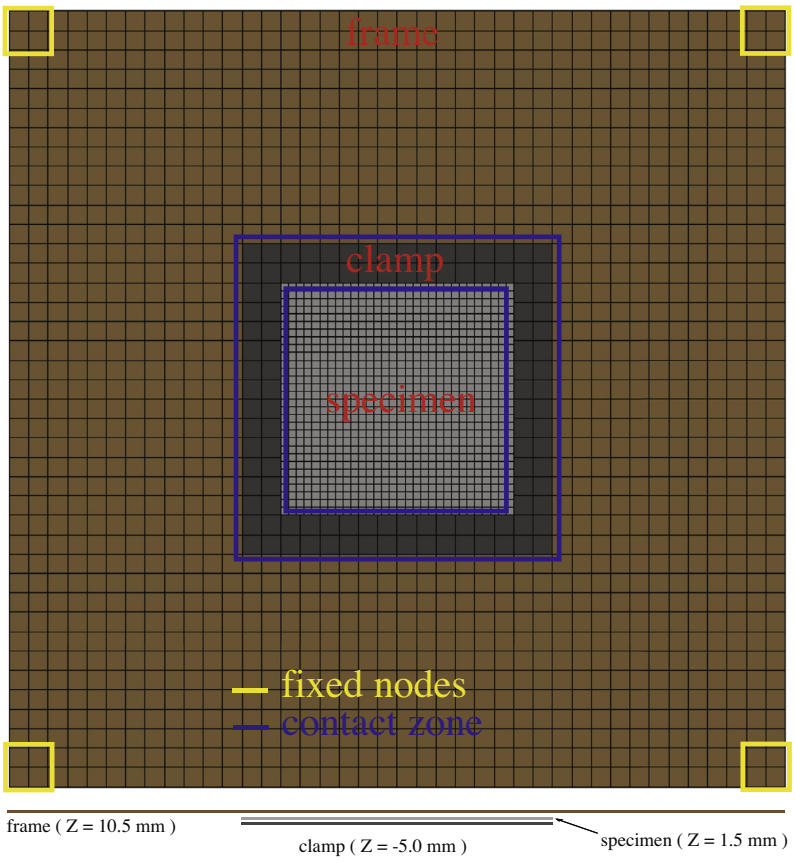

Fig. 2. Finite element model.

clamping frame (dark gray) with dimensions according to the values provided in Section 2. The three parts contain, respectively, 1600, 1456 and 112 quadrilateral Lagrangian shell elements (Belytschko–Lin–Tsay shell elements (LSTC, 2007). Fixed boundary conditions are applied at the four corners of the steel mounting frame. A tied nodes-to-surface contact algorithm with offset is implemented to model the interaction between the different parts. The nodes of the specimen in the blue area (slave nodes) are tied to the steel frame and the aluminum clamp which both act as master surface. For all parts, the middle surface is chosen as the reference surface. Therefore, the offset of the three shell parts needs to be considered.

4. Material models

In this article the von Mises yield criterion (also referred to as the Huber–Hencky-von Mises criterion) is used to describe the yield surface. Three different phenomenological models are used to describe the strain and strain rate hardening of aluminum assuming the hardening as isotropic.

The first empirical model used in this article to describe the hardening behavior of the aluminum plate is a combination of the simple linear strain hardening model with the strain rate term of the Cowper–Symonds (Cowper and Symonds, 1957) model:

$$\bar{\sigma}_Y = \left[\sigma_0 + E_p \bar{\varepsilon}^{\mathrm{pl}}\right]\left[1 + \left(\frac{\dot{\varepsilon}}{C}\right)^{1/P}\right] \tag{2}$$

where σ_0 is the initial yield stress, $\bar{\varepsilon}^{\mathrm{pl}}$ the equivalent plastic strain, E_p is regarded as the plastic hardening modulus, $\dot{\varepsilon} = \sqrt{\dot{\varepsilon}_{ij}\dot{\varepsilon}_{ij}}$ the total strain rate and C, P are strain rate parameters. This model will be abbreviated in this article as linH–CS.

The second empirical model is the one proposed by Johnson and Cook (1983) and is expressed as follows:

$$\bar{\sigma}_Y = \left[A + B\left(\bar{\varepsilon}^{\mathrm{pl}}\right)^n\right]\left[1 + C\ln\frac{\dot{\bar{\varepsilon}}^{\mathrm{pl}}}{\dot{\varepsilon}_0}\right] \tag{3}$$

where $\bar{\varepsilon}^{\mathrm{pl}}$ is the equivalent plastic strain, $\dot{\bar{\varepsilon}}^{\mathrm{pl}}$ equivalent plastic strain rate and $\dot{\varepsilon}_0 = 1.0\ s^{-1}$ the reference strain rate (quasi-static). The four material constants are A, B, n and C. The expression in the first set of brackets gives the equivalent yield stress as a function of strain for $\dot{\bar{\varepsilon}}^{\mathrm{pl}} = 1.0\ s^{-1}$. The expression in the second set of brackets represent the effect of strain rate. This model will be abbreviated in this article as J–C. It should be noted that the general Johnson–Cook model includes effects of thermal softening by an additional scale factor. The temperature effects on the yield stress are negligible for this specific problem as the increase due to adiabatic heating is less than one degree.

In addition to the previous models, a third phenomenological model is used according to experimental data from uniaxial tensile tests on aluminum T-bone specimens performed by the authors. The model is constructed by combining a strain hardening term described by a bi-exponential relation (adapted hyperbolic tangent function) and the strain rate hardening term of the Cowper–Symonds model:

$$\bar{\sigma}_Y = \left[K_1 e^{K_2\bar{\varepsilon}^{\mathrm{pl}}} + K_3 e^{K_4\bar{\varepsilon}^{\mathrm{pl}}} + (\sigma_0 - K_1 - K_3)\right]\left[1 + \left(\frac{\dot{\varepsilon}}{C}\right)^{1/P}\right] \tag{4}$$

where σ_0 is the initial yield stress, $\bar{\varepsilon}^{\mathrm{pl}}$ the equivalent plastic strain, $\dot{\varepsilon}$ the total strain rate, K_1, K_2, K_3 and K_4 parameters describing the

hardening behavior and C and P describing the strain rate behavior. This model will be abbreviated in this article as expH–CS.

5. Material identification through inverse methods

The basis for material identification is the fundamental assumption that the outcome of some measurements on the response of the material can be predicted through a physical law. The problem of predicting the result of measurements is called the *simulation* or *forward* problem. The *inverse* problem consists of using the actual result of the measurements to infer the values of the parameters that characterize the material. Inverse problems may be difficult to solve for at least two different reasons:

1. Different values of the model parameters may be consistent with the data.
2. Discovering the values of the model parameters may require the exploration of a huge parameter space.

A special class of inverse methods for material identification are the so-called *Mixed Numerical Experimental Techniques* (MNETs) introduced first by Kavanagh and Clough (1971). These methods are based on numerical solutions for the prediction of the deformation field and they approach the identification problem through the minimization of the residual between the numerically predicted and experimentally observed responses (also known as cost function). According to the list of Avril et al. (2008), the most widely used identification methods for material identification are:

1. The *FE Model Updating Method* (FEMU) which is based on the minimization of the discrepancy between the experimental and the numerical displacement fields described by a weighted least square formulation (Cooreman et al., 2007; Lecompte et al., 2007; Lecompte et al., 2005; Molimard et al., 2005; Mauvoisin et al., 1994; Moreau et al., 2006; Pagnacco et al., 2007; Cooreman et al., 2008; Genovese et al., 2006).
2. The *Constitutive Equation Gap Method* (CEGM) which is based on the minimization of a constitutive equation gap functional (Constantinescu, 1995; Geymonat et al., 2002; Geymonat and Pagano, 2003; Latourte et al., 2008; Hadj-Sassi and Andrieux, 2007; Nguyen et al., 2006).
3. The*Virtual Fields Method* (VFM) based on the virtual work principle applied on well-chosen virtual fields. The aim is to minimize the difference between the internal and the external virtual work of the system (Grédiac and Pierron, 2006; Chalal et al., 2006; Avril et al., 2008; Avril et al., 2008).
4. The *Equilibrium Gap Method* (EGM) based on the minimization of the equilibrium gap (Bui, 1995; Ikehata, 1990).
5. The *Reciprocity Gap Method*(RGM) based on the Maxwell–Betti reciprocity theorem and adjoint fields. The material parameters are identified by minimizing the reciprocity gap for any adjoint field (Calderon, 1980; Andrieux et al., 1997; Abda et al., 1999; Bui et al., 2004).

In this article the FE method is needed to numerically simulate the dynamic blast response of the aluminum plate specimen. Therefore, the finite element based inverse method (FEMU method) using a gradient based optimization is adopted. More precisely, the Levenberg–Marquardt (L–M) solution (a damped least-squares method) is used to the minimize the cost function of the least squares problem. It provides a stable numerical solution to the problem of minimizing a function over a space of parameters of the function in least squares curve fitting and nonlinear programming. Details on the L–M algorithm are available in Levenberg (1944) and Marquardt (1963).

6. Identification of the plastic behavior of aluminum plates using inverse methods

This section presents the results of the parameter identification for the three proposed strain hardening models described in Section 4. First, virtual measurement data through a *virtual experiment* is generated with the finite element method in order to validate the identification process numerically. Next, the sensitivity to measurement uncertainties is investigated by adding normally distributed noise (Gaussian noise) to the virtual experiment. Finally, the plastic behavior of aluminum is identified using real experimental data obtained from controlled detonation of C4 as described in Section 2.

6.1. Efficiency of the identification process through virtual experiments

A damped Levenberg–Marquardt algorithm is applied to minimize the non-linear least squares problem. To build the objective function, the in-plane true strain fields ε_{xx} and ε_{yy} are chosen as response values. For a faster solution of the inverse problem it is beneficial to use the strain components as they are more sensitive to changes of the material parameters. The strain components are obtained from 400 points according to the following grid positions: x from -95 mm to 95 mm (step: 10 mm) and y from -95 mm to 95 mm (step: 10 mm), corresponding to the integration points of the shells elements (upper surface). Reading out data throughout a grid assures the spatial alignment. To identify the strain hardening parameters, only time steps including material yielding should be taken into account during optimization. These time steps contain sufficient information with respect to the material parameters, and therefore sensitivity is assured. Plasticity is occurring in the beginning of the blast response. Therefore, only response data between 0.24 ms and 0.68 ms are used in the inverse loop.

To end the optimization loop a convergence criterion is necessary. The convergence criterion is based on the relative difference of the values of the parameters in the current and in the previous iteration:

$$D_k = \left| \frac{p_j^k - p_j^{k-1}}{\frac{\left(p_j^k + p_j^{k-1}\right)}{2}} \right| \tag{5}$$

For the results presented in this article the identification process is terminated when the relative difference of all the parameters is lower than or equal to 0.1 %. Furthermore, the components of the sensitivity matrix, *i.e.* Jacobian matrix **J**, are calculated numerically as forward finite differences:

$$J_{i1} = \frac{\hat{\boldsymbol{\varepsilon}}_i(\mathbf{p}, p_1 + dp_1) - \hat{\boldsymbol{\varepsilon}}_i(\mathbf{p}, p_1)}{dp_1} \tag{6}$$

with J_{i1} the sensitivity column of parameter p_1, dp_1 the finite difference of parameter p_1 and $\hat{\boldsymbol{\varepsilon}}_i(\mathbf{p})$ the response of the solution to the direct problem using a given set of parameters **p**. The size of the finite differences is investigated by evaluating the condition number of the sensitivity matrix. This number should be as close as possible to 1 to obtain a fast and stable convergence. More details on this method can be found in Cooreman et al. (2008) and Lecompte (2007).

The optimization algorithm is numerically validated for the three different hardening models. All models present a stable convergence and the material parameters converge to the correct values of the virtual experiment. Results for the linH–CS model (see Eq. (2)) are presented here. The virtual experiment is generated using the following set of material parameters: $\sigma_0 = 0.083$ GPa, $E_p = 3.6$ GPa, $C = 6.5\ (\text{ms})^{-1}$ and $P = 4$. During optimization, four

material parameters are identified starting with initial parameter values $\sigma_0 = 0.1$ GPa, $E_p = 1$ GPa, $C = 1\ (\text{ms})^{-1}$ and $P = 1$. Fig. 3 illustrates the convergence path of all parameters. The plots show that convergence for all parameters is obtained after nine iterations. For each step in the iterative process, five successive FE-simulations are necessary: one simulation with the current set of material parameters and four additional simulations to calculate each parameter sensitivity. Accordingly, a total of forty five simulations are needed to attain convergence for all parameters. The convergence of the parameters is clearly visible by plotting the objective function as a function of the iteration steps (see Fig. 4).

6.2. Virtual experiment with Gaussian noise

A measurement under ideal conditions has no errors. However, real measurement results will always contain measurement errors of varying magnitudes. A systematic and systemic approach is needed to identify every possible source of error that can arise within a given measuring system. It is then necessary to describe their magnitude as well as their impact on the prevailing operational conditions.

The measurement error is defined as the difference between the distorted and the undistorted information about a measured object, expressed in its measurands. The measurement errors are classified into systematic and random errors. Systematic errors refer to permanent deflection in the same direction from the true value and they are related to the accuracy of the measurement. These errors can be controlled by monitoring measurements against a check standard over time. In contrast, random errors refer to short-term scattering of values around a mean value and they are related to the precision of the measurement. They cannot be corrected on an individual measurement basis but they can be approximated by statistical models.

In this article the investigation is concentrated on the random error from DIC measurements. It has been reported that the random error on the strain components can be statistically approximated through a Gaussian distribution and therefore, it can be formulated as standard error (Sutton et al., 2009). In this section the influence of the standard error to the identification process is investigated by adding noise on the strain components computed from the virtual experiment. Two different levels of noise are considered: Gaussian noise with standard deviation of 100 μstrain and Gaussian noise with standard deviation of 200 μstrain (both noises are normalized to a mean alue of $\mu = 0$ μstrain, see Fig. 5). It should be noticed that the accuracy of the 3D-DIC system adopted in the article is in the order of magnitude of 200 μstrain (Becker et al., 2006; Schreier et al., 2006).

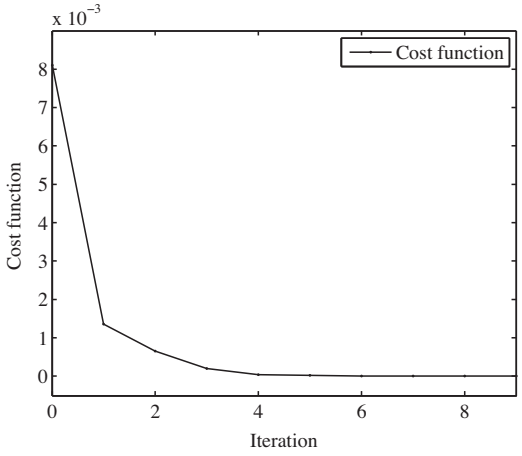

Fig. 4. Evolution of the objective function during the identification process. The objective function is gradually reduced and finally converges to its minimum value.

Tables 1–3 present the relative errors on the obtained material parameters for two levels of noise, respectively for the linH–CS, J–C and expH–CS model. The identified values are obtained by averaging the results of seven identification processes. For unbiased virtual data (zero noise) the identified parameters converge to the assumed 'real' values. In this case, a perfect fit of the parameters is expected as far as the same finite element formulation is used for the numerical and the experimental (virtual) part of the process. For noise of 100 μstrain the parameters of all the three models present small deviations from the assumed 'real' values. The

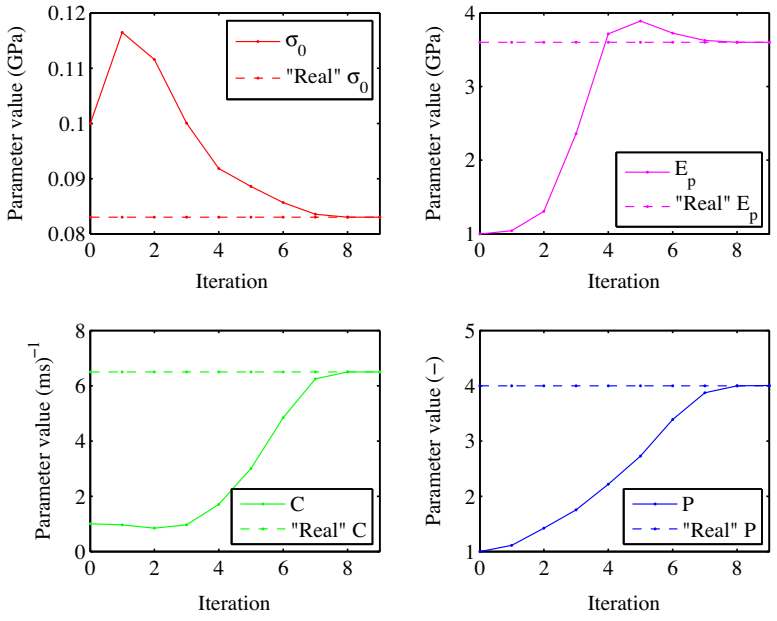

Fig. 3. Convergence paths of the four parameters of the combined linear strain hardening model with the strain rate term of the Cowper–Symonds model based on measurements obtained from a virtual experiment. After nine iterations all the parameters have converged to the 'real' values.

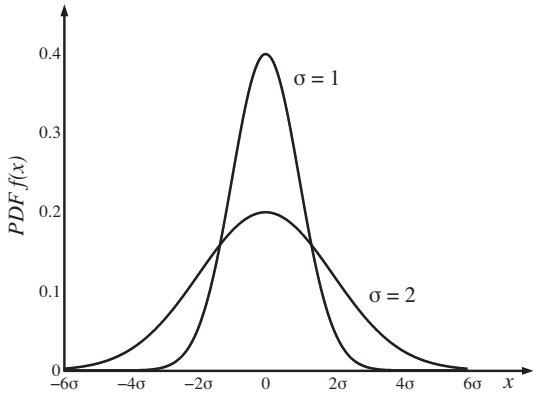

Fig. 5. Normal distribution. Probability density function (PDF) $f(x)$ vs. support x.

relative errors are in the order of magnitude of 0.2–3.0% and therefore the efficiency of the identification process remains high. For noise of 200 μstrain the deviation on the obtained parameters of all the three models is increased. Notice that for the linH–CS model and the J–C model the relative errors vary from 0.1 to 1.7%. Hence, the efficiency of the identification process remains high. However, for the expH–CS model relative errors up to 6.5% are obtained. Therefore, it can be concluded that in terms of measurement noise, the expH–CS model presents the highest sensitivity among all the examined models.

6.3. Real experiment

The main purpose of this article is the identification of the plastic behavior of aluminum under blast loading according to the experimental setup described in Section 2. The identification is repeated for four identical experiments. For the identification process the three phenomenological hardening laws are considered according to Eqs. (2)–(4). The identification routine is based on the Levenberg–Marquardt algorithm.

Apart from the error introduced by the strain measurements, a second source of error during the identification process is the asymmetry of the actual blast wave. This asymmetry is mainly caused by two factors. The first factor is the poor positioning of the explosive charge with respect to the normal axis of the center point of the plate (theoretical position: x = 0 mm, y = 0 mm). The second factor is related to the shape of the explosive (theoretically spherical) and the position of the detonator (theoretically in the center of the explosive mass). Consequently, the dynamic response of the plate is not exact symmetrical regarding to the central axis. More details about the observed asymmetry can be found in the previous work of the authors (Spranghers et al., 2012). However, ConWep is based on the assumption that the free air blast wave is perfectly symmetrical in space. Due to this limitation, the positioning of the explosive charge is considered as the only possible source of error for this work. In order to investigate the influence of the explosive's position, the identification process is enhanced with two extra parameters, *i.e.* the coordinates of the explosive's location (in the X–Y plane).

To take into account the uncertainty on the explosive's location, a two-stage identification process is followed. In the first stage, the coordinates of the explosive's location are identified through the displacement fields extracted from the first time steps (from 0.12 ms to 0.24 ms) of the elastic deformation of the plates. In the second stage, the plastic behavior of the aluminum plates is identified according to the strain fields captured from 0.24 ms to 0.68 ms where plasticity is observed. The use of the displacement

Table 1
linH–CS model with Gaussian noise (μ = 0 μstrain).

σ_{noise}		σ_0 (GPa)	E_p (GPa)	C (ms)$^{-1}$	P (-)
0 μs	Identified values	8.30×10^{-2}	3.60	6.50	4.00
	Relative error	0%	0%	0%	0%
100 μs	Identified values	8.28×10^{-2}	3.59	6.52	4.04
	Relative error	0.24%	0.28%	0.31%	1.00%
200 μs	Identified values	8.32×10^{-2}	3.61	6.39	3.95
	Relative error	0.24%	0.28%	1.71%	1.26%

Table 2
J–C model with Gaussian noise (μ = 0 μstrain).

σ_{noise}		A (GPa)	B (GPa)	n (-)	C (-)
0 μs	Identified values	11.00×10^{-2}	15.00×10^{-2}	36.00×10^{-2}	14.00×10^{-3}
	Relative error	0%	0%	0%	0%
100 μs	Identified values	10.98×10^{-2}	14.97×10^{-2}	35.79×10^{-2}	13.93×10^{-3}
	Relative error	0.18%	0.20%	0.59%	0.50%
200 μs	Identified values	11.01×10^{-2}	15.23×10^{-2}	36.38×10^{-2}	13.97×10^{-3}
	Relative error	0.09%	1.52%	1.05%	0.21%

Table 3
expH–CS model with Gaussian noise (μ = 0 μstrain).

σ_{noise}		K_1 (GPa)	K_2 (-)	K_3 (GPa)	K_4 (-)	C (ms)$^{-1}$	P (-)	σ_0 (GPa)
0 μs	Identified values	-38.00×10^{-3}	−1232	-11.00×10^{-3}	−140.0	6.50	2.00	9.00×10^{-2}
	Relative error	0%	0%	0%	0%	0%	0%	0%
100 μs	Identified values	-37.90×10^{-3}	−1236	-11.16×10^{-3}	−140.4	6.71	2.02	8.98×10^{-2}
	Relative error	0.26%	0.32%	1.44%	0.29%	3.18%	1.00%	0.22%
200 μs	Identified values	-37.89×10^{-3}	−1266	-11.56×10^{-3}	−148.5	6.09	1.97	8.95×10^{-2}
	Relative error	0.29%	2.72%	4.96%	5.89%	6.51%	1.51%	0.56%

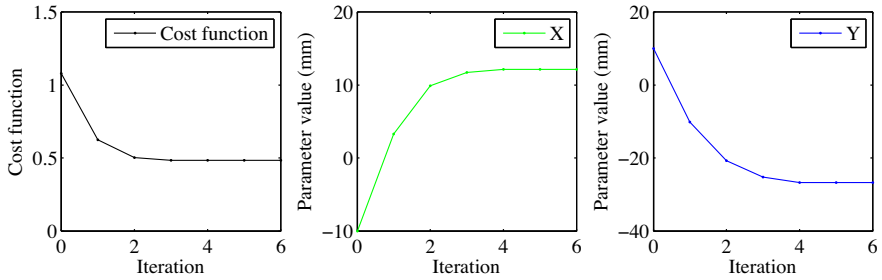

Fig. 6. Evolution of the cost function and the convergence path of the coordinates of the explosive's location for experiment 1.

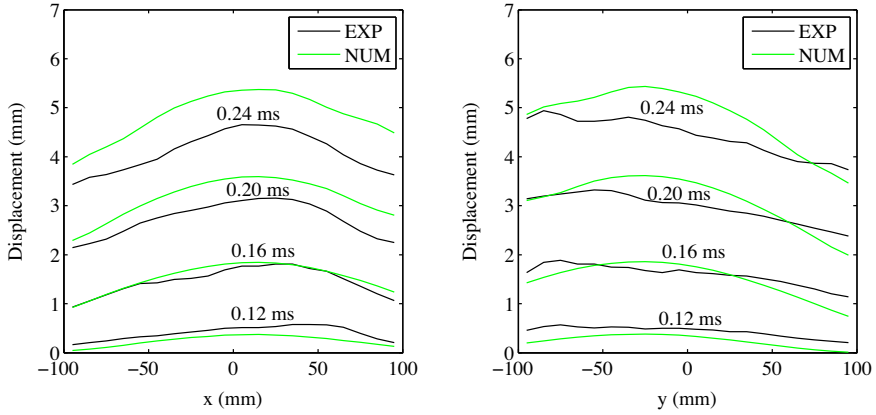

Fig. 7. Out-of-plane displacement profiles along the X-axis (left) and Y-axis (right) of the plate at early stages of the deformation for experiment 1.

fields instead of the strain fields for the identification of the explosive's location is based on the fact that at very early stages, the displacement of the plate is dominated by high rigid movements due to the imparted momentum, while the amplitudes of strain fields remain low. Fig. 6 shows, for the case of experiment 1, the convergence path of the coordinates of the explosive's location as well as the evolution of the cost function. Although different starting values for the coordinates are used, the identified coordinates converge the same values. Similar results are obtained for the remaining three experiments. More precisely, for experiment 1 the identified coordinates are: x = 13.02 mm, y = −27.80 mm, for experiment 2: x = −13.72 mm, y = −8.97 mm, for experiment 3: x = 79.22 mm, y = −35.76 mm and for experiment 4: x = 0.76 mm, y = 4.97 mm. Notice that a significant difference is observed between the results of the four experiments and therefore the location of the detonation point is a crucial factor for the identification of the material parameters. The importance of the location of the detonation point is plotted in Fig. 7 where at the early stages of the deformation (elastic) the correction of the detonation point provides a better agreement with the experimentally observed asymmetric response.

In order to highlight the effect on the explosive's location to the accuracy of the identification of the plastic behavior, the results include two scenarios. The first scenario assumes that the explosive's location is a priori known and fixed to the theoretical position (x = 0 mm, y = 0 mm) while the plastic behavior is the only item that the identification process aims to identify. The second scenario includes the identification of both the explosive's location and the plastic hardening parameters.

The complex expH–CS model (see Eq. (4)) is selected in order to visualize the capability of inverse methods to simultaneously identify the total set of parameters though a single experiment. Notice that the expH–CS model requires the identification of 7 parameters. Similar results are obtained for the remaining two models. Fig. 8 shows the convergence paths of the parameters for the expH–CS model. It plots the following two cases: (a) the detonation point is assumed known and fixed and (b) the detonation point is included in the identification process as extra unknown parameter. For both cases a total of 18 iterations are needed to attain convergence for all parameters with a total computational time of 1 h 21 min and 1 h 32 min, respectively. It can be noticed that the inclusion or exclusion of the detonation point has a significant effect on the identified values of the material parameters. The value of the cost function indicates the level of efficiency of the two identification procedures. The exclusion of the detonation point from the identification process yields a cost function with a minimum value of 0.044 whereas inclusion of the detonation point leads to a significantly lower value of 0.039. Therefore, it can be concluded that the addition of the detonation point as extra unknown parameter in the identification process will increase the accuracy of the identified material behavior. This is highlighted in Fig. 9 where the out-of-plane displacement profiles are plotted for cases (a) and (b). The inclusion of the detonation point in the identification process provides a more accurate prediction of the blast response since the effect of wave asymmetry is taken into account.

The same process was followed for the two remaining models (linH–CS and J–C) but for space-saving purposes the convergence paths are not presented. Instead, Tables 4–6 give the identified values for each model with and without the determination of the detonation point. Fig. 10 presents the equivalent stress–strain curves for the three identified models based on the four experiments at a strain rate of 100 s^{-1} (note that the maximum strain rate obtained during the four experiments is in the same order of magnitude). It is clear that the first hardening model (linH–CS) is less adequate in approximating the real hardening behavior. This can be explained by the functional form of the model which has only two parameters to describe the strain hardening for a certain strain rate, *i.e.* the initial yield point σ_0 (constant term) and the hardening

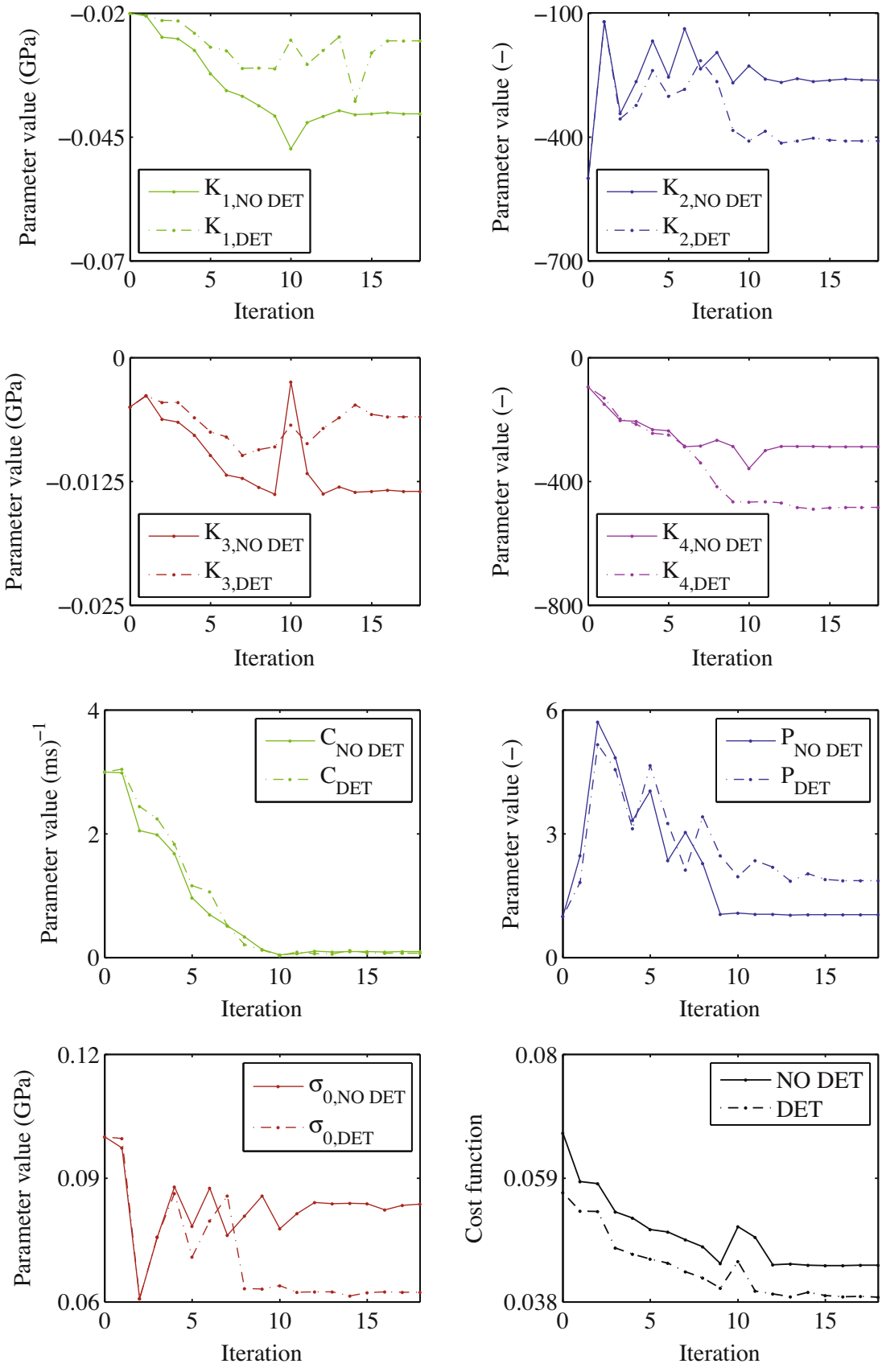

Fig. 8. Convergence paths of the parameters for the expH–CS model and evolution of the cost function for experiment 1.

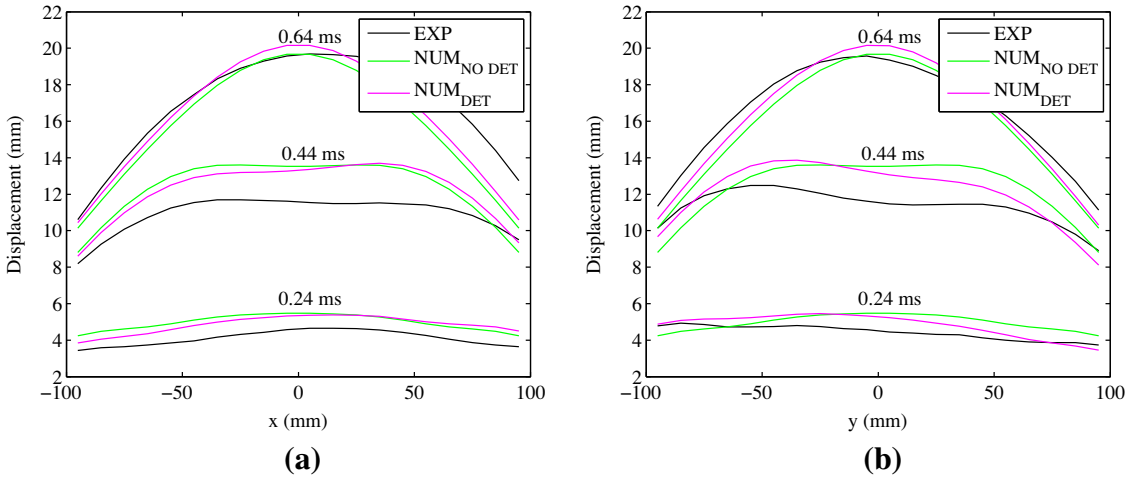

Fig. 9. Out-of-plane displacement profiles: (a) along the X-axis and (b) along the Y-axis (experiment 1).

modulus E_p (the slope). Therefore, this model is less capable to approximate the strain hardening in the beginning of the hardening process where the slope is decreasing as the strain increases. The output of the identification action is always affected by measurement and modelization uncertainties. In Section 6.2 the influence of measurement noise is investigated using a virtual experiment superposed with Gaussian noise (with the same order of magnitude as the resolution of the measurement system). Results show that in the efficiency of the identification process remains high. However, for real experimental data the choice of

Table 4
Material parameter identification (linH-CS).

	Detonation point	σ_0 (GPa)	E_p (GPa)	C (ms)$^{-1}$	P (-)	cost (-)
EXP 1	without	0.079	1.26	0.041	1.05	0.0414
	with	0.082	0.62	0.050	1.34	0.0376
EXP 2	without	0.061	5.50	0.027	1.88	0.0346
	with	0.079	3.66	0.043	1.18	0.0323
EXP 3	without	0.067	5.94	0.037	1.27	0.0454
	with	0.076	0.01	0.043	1.18	0.0322
EXP 4	without	0.091	0.73	0.026	1.00	0.0399
	with	0.085	2.34	0.026	1.00	0.0400

Table 5
Material parameter identification (J–C).

	Detonation point	A (GPa)	B (GPa)	n (-)	C (-)	cost (-)
EXP 1	without	0.0405	0.0102	0.309	0.758	0.0416
	with	0.0503	0.0275	0.362	0.512	0.0376
EXP 2	without	0.0386	0.0106	0.305	0.929	0.0335
	with	0.0480	0.0108	0.327	0.688	0.0314
EXP 3	without	0.0306	0.0642	0.351	1.000	0.0454
	with	0.0317	0.0101	0.204	0.890	0.0325
EXP 4	without	0.0270	0.1249	0.526	1.599	0.0409
	with	0.0291	0.1856	0.543	1.327	0.0411

Table 6
Material parameter identification (expH–CS).

	Detonation point	K_1 (GPa)	K_2 (-)	K_3 (GPa)	K_4 (-)	C (ms)$^{-1}$	P (-)	σ_0 (GPa)	cost (-)
EXP 1	without	−0.0403	−262.12	−0.0135	−287.49	0.0949	1.037	0.0837	0.0443
	with	−0.0256	−409.42	−0.0060	−484.38	0.0689	1.860	0.0624	0.0388
EXP 2	without	−0.0381	−184.47	−0.0062	−394.74	0.0917	1.639	0.0883	0.0368
	with	−0.0355	−192.17	−0.0112	−319.86	0.1026	1.495	0.0906	0.0343
EXP 3	without	−0.0437	−148.25	−0.0133	−341.53	0.0924	1.645	0.0887	0.0491
	with	−0.0309	−450.47	−0.0141	−389.83	0.0707	1.299	0.0559	0.0325
EXP 4	without	−0.0340	−265.79	−0.0029	−343.78	0.1046	1.375	0.1355	0.0475
	with	−0.0361	−236.31	−0.0179	−330.53	0.0989	1.092	0.1251	0.0460

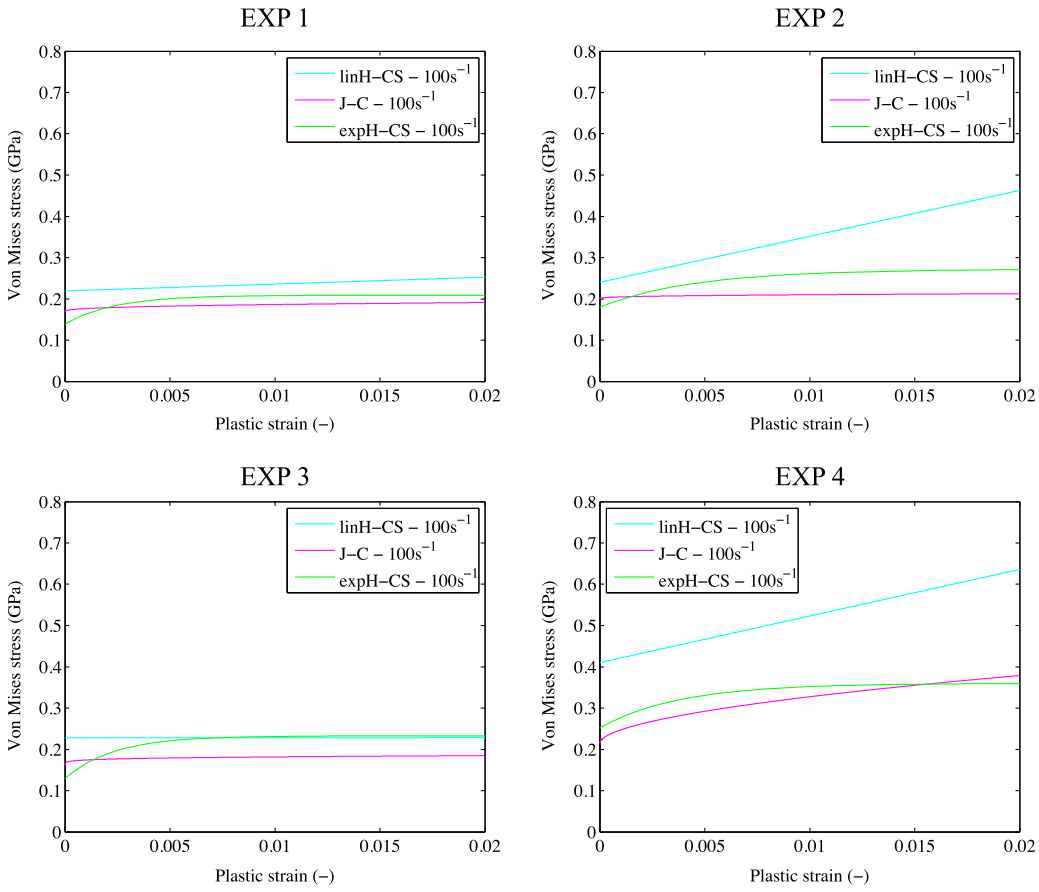

Fig. 10. The equivalent stress–strain curves, at a strain rate of 100 s^{-1}, for the three identified models based on the four experiments.

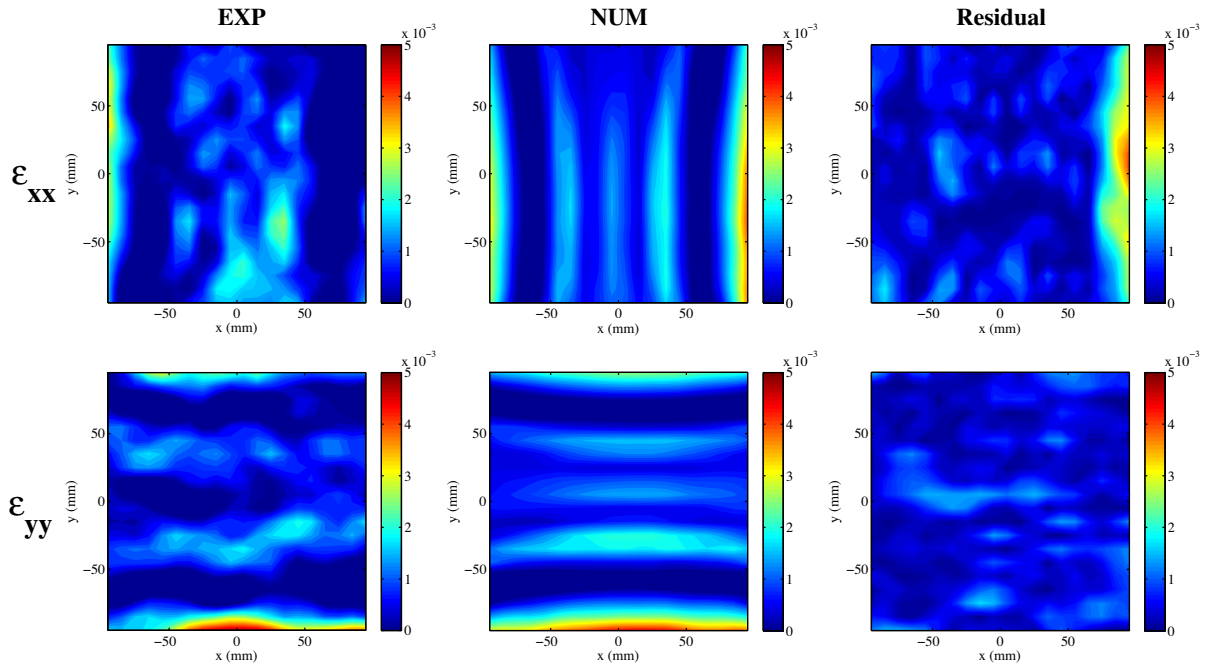

Fig. 11. In-plane true strain ε_{xx} and ε_{yy} at 0.24 ms: experimental *vs.* numerical (experiment 1).

the hardening model is of the utmost importance. If the model is not capable of approximating the actual behavior, the uncertainty on the identified parameters is increased.

It is clear that the efficiency of the identified material model is closely related to the accurate modeling of the experimental conditions. Figs. 11–13 present the experimental strain fields extracted

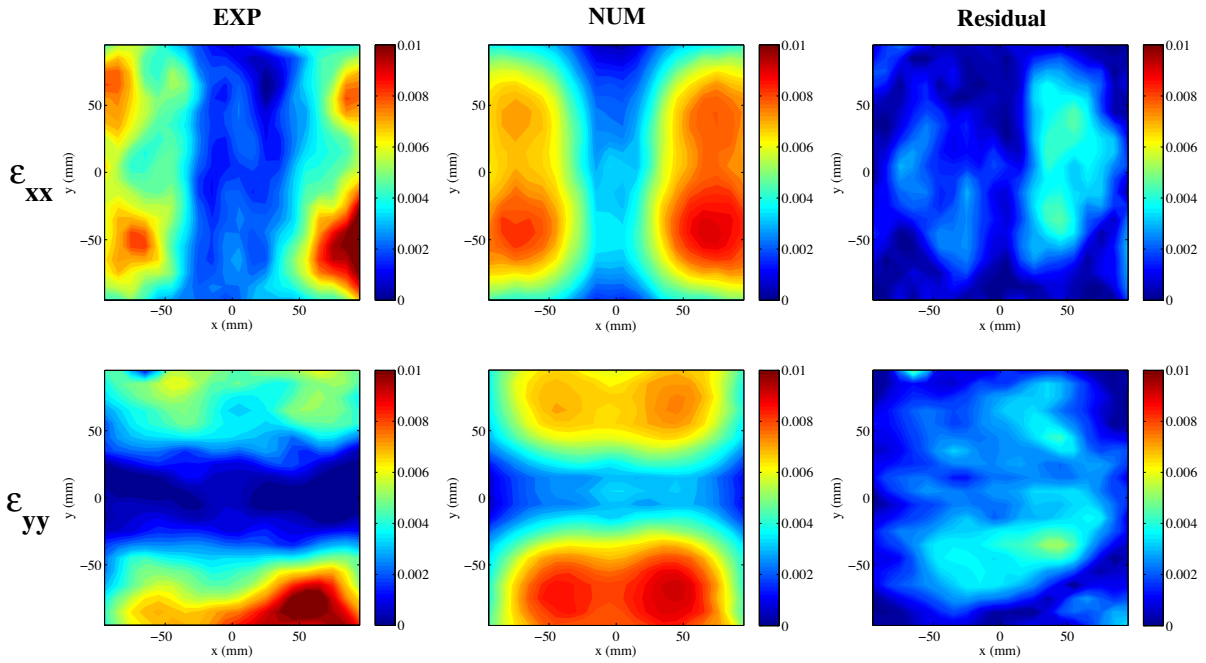

Fig. 12. In-plane true strain ε_{xx} and ε_{yy} at 0.44 ms: experimental *vs.* numerical (experiment 1).

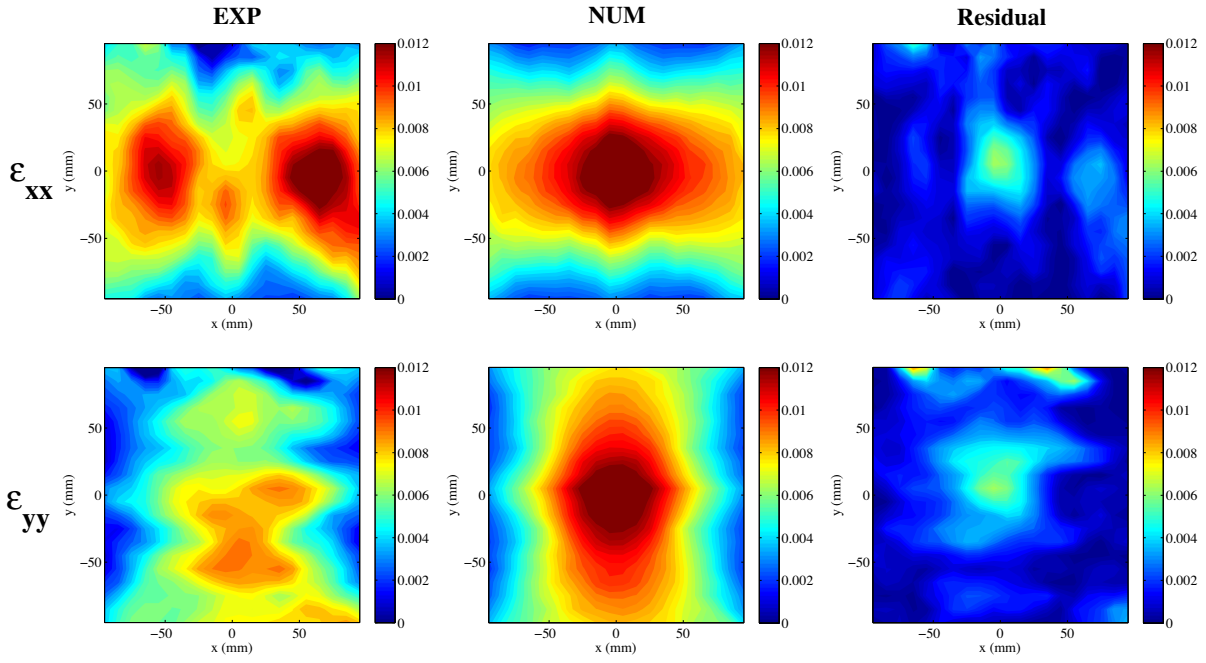

Fig. 13. In-plane true strain ε_{xx} and ε_{yy} at 0.64 ms: experimental *vs.* numerical (experiment 1).

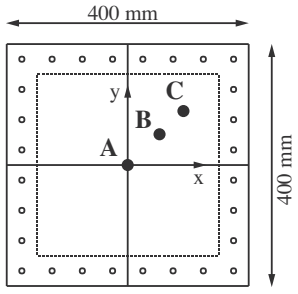

Fig. 14. Coordinates on the plate specimen: A (0,0), B (55,55) and C (95,95).

from the 3D-DIC system, those computed from the numerical model as well as the residuals for three different time steps (respectively, 0.24 ms, 0.44 ms and 0.64 ms). An important correlation between the experimental and the numerical strain fields is observed.

It was mentioned in previous sections that for this article three different phenomenological plastic models are considered. To evaluate the ability of each identified model to predict the actual response, the out-of-plane displacement and the two true in-plane strain components are plotted as a function of time in three different points of the testing plate. Point A corresponds to the central

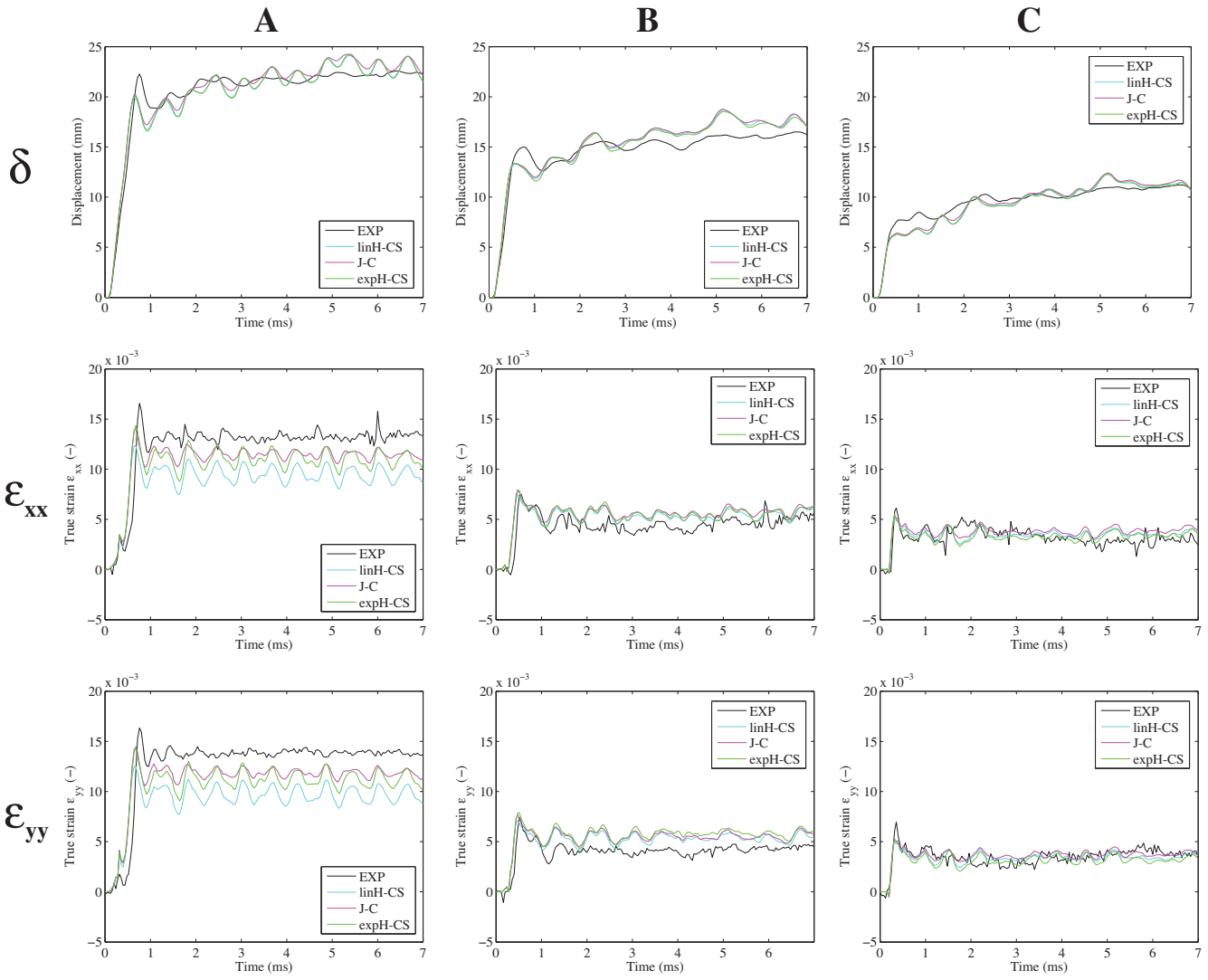

Fig. 15. History plots: out-of-plane displacement δ, true in-plane strain ε_{xx} and true in-plane strain ε_{yy} (experiment 1).

Table 7
Computed SSR-values.

	EXP 1	EXP 2	EXP 3	EXP 4
J–C: Identified	0.0381	0.0327	0.0338	0.0419
J–C: Literature	0.0522	0.0605	0.0657	0.0825
Tensile Test	0.0477	0.0503	0.0567	0.0664

point of the plate and the remaining two (point B and C) are located on the diagonal (see Fig. 14). It can be seen from Fig. 15 that all the three models provide similar responses close to the experimentally observed responses. However, in terms of strains it can be noticed that the J–C model provides a slightly better prediction of the actual response, especially on the central point where a maximum deformation occurs.

The final aim of this study is to compare the ability of the numerical model to predict the actual blast response for strain hardening behavior obtained from the current inverse method, from literature and finally from uniaxial tensile tests performed by the authors. For the comparison, the J–C model will be presented. The identified parameter values for the current inverse method are available in Table 5 (with detonation point included). The parameters values from literature are presented here:

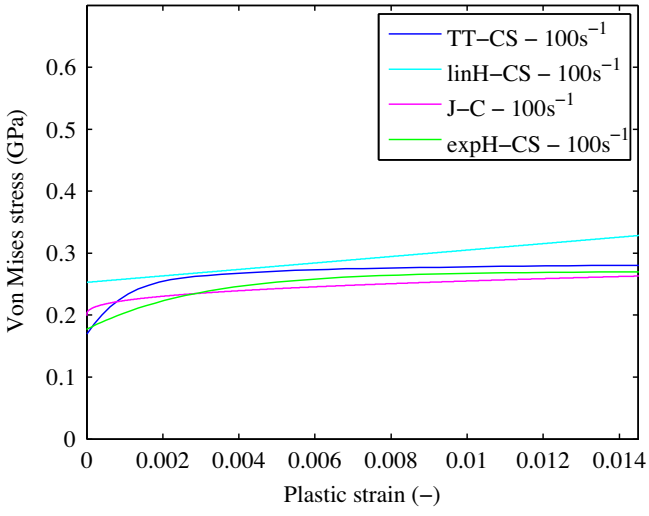

Fig. 16. Comparison of the equivalent stress–strain curves from the identification with the stress–strain curve from uniaxial tensile tests (strain rate of 100 s^{-1}).

$A = 0.110$ GPa, $B = 0.150$ GPa, $n = 0.360$ and $C = 0.014$ (Christoulis et al., 2011). For the uniaxial tensile tests, the equivalent stress–strain response (the average of 8 specimens) is directly implemented in the numerical model as plastic behavior and strain rate effects are included using the strain rate term of the Cowper–Symonds model with strain rate parameters from literature: $C = 6.5\ (\text{ms})^{-1}$ and $P = 4$ (Jones, 1989).

The most efficient way to compare the predicted with the actual response is to compute the sum of squared residuals (SSR). It is a statistical measure of the discrepancy between the experimental measurements and an estimation model. The lower the SSR-value the better the prediction of the numerical model. The SSR-value is computed as follows:

$$\text{SSR} = \sum_{t=t_1}^{t_m}\sum_{i=1}^{n}\left(\boldsymbol{\varepsilon}_{t,i}^{\text{exp}} - \boldsymbol{\varepsilon}_{t,i}^{\text{num}}(\mathbf{p})\right)^2 \tag{7}$$

where $\boldsymbol{\varepsilon}_{t,i}^{\text{exp}}$ is a vector containing the experimental strain components of the i-th point of the aluminum plate at time t and $\boldsymbol{\varepsilon}_{t,i}^{\text{num}}(\mathbf{p})$ the vector of the computed strains in the same point for material parameters $\mathbf{p}$. It can be noticed from Table 7 that the numerical model based on the strain hardening behavior identified by the inverse method, is presenting the lowest-SSR value for all the four experiments. More precisely, it presents respectively for the four experiments a 20%, 35%, 40% and 37% lower SSR-value than the numerical model based on hardening behavior obtained by uniaxial testing and a 27%, 46%, 49% and 49% lower SSR-value than the numerical model based on hardening behavior obtained from literature. According to the results, it can be concluded that the use of inverse methods for the direct identification of the strain hardening behavior through the actual experimental setup allows for a prediction of the measured material response.

Fig. 16 compares the resulting strain hardening curves from the identification with the hardening curve from quasi-static uniaxial tension tests. For the identified curves the average of the identified parameter sets from the four experiments is used. The plot presents the comparison for a strain rate of 100 s^{-1}. During the tensile tests the specimens are loaded quasi-statically, meaning no strain rate information can be derived. Therefore, the identified Cowper–Symonds strain rate parameters from the expH–CS model are used to include strain rate effects. Results show that the stress–strain curves from the three different hardening models are consistent with the results from the uniaxial tensile tests.

7. Conclusions

The present article introduces the use of inverse methods for the identification of the plastic behavior of aluminum plates subjected to free air explosions. The main purpose of the authors is to show that the use of full-field high-speed optical measurements and finite element modeling allows the direct identification of the material response without the need of additional testing. A free air blast load makes it possible to load a plate specimen at different strains and strain rates in different zones. This makes the test suitable for material identification using inverse methods, which profit from heterogeneous displacement and strain fields.

For the identification of the plastic behavior of aluminum a methodology is presented based on the minimization of the squared residuals between the experimentally measured and numerically computed strains. To ensure the stability of the identification a damped least-squared solution is applied according to the Levenberg–Marquardt formulation. Three phenomenological laws, starting from a simple linear model to the well-known Johnson–Cook model and a complex bi-exponential expression for the strain hardening, are considered. The purpose is to show that the efficiency of the identification process is independent from the complexity of the hardening model. It is proven that the identification process is capable, for all the three considered models, to converge to a stable solution. This reinforces the fact that inverse methods can be successfully used for the determination of the material parameters as far as complex heterogenous deformation fields are available.

A major concern when applying material identification is the effect of possible sources of errors that may cause significant loss of accuracy on the obtained parameter values. In this article two types of errors are investigated. The first error is related to the measurement uncertainties of the 3D-DIC system. To investigate the influence of this type of error on the efficiency of the identification process a series of virtual experiments are performed. The assumed 'experimental' strains are superimposed with two different levels of Gaussian noise, *i.e.* 100 μstrain and 200 μstrain. It is shown that the inverse method presents very low sensitivity to these levels of noise and therefore it is concluded that the use of the DIC system as measuring instrument is a preferable choice for this type of experiments. The second type of error is the uncertainty on the location of the explosive's detonation point in the numerical simulation. It is highlighted in this article that poor positioning fails to predict the actual experimentally observed asymmetry of the blast response. To overcome this problem, the authors present a two-step identification process where the location of the detonation point is added as extra unknown to the set of material parameters. The results show that inclusion of the explosive's location as extra parameter to the identification process increases the accuracy of the predicted blast response and improves the quality of the identification action.

The numerical simulations, using the three different hardening models combined with the identified material parameter values based on real experimental measurements, provide similar responses close to the experimentally observed responses. To examine the efficiency of the results, the predicted response of the plate using strain hardening behavior obtained from the current inverse method is compared with the predicted responses using strain hardening behavior from literature as well as obtained from uniaxial tensile testing. It is shown in the results that the output of the identification process presented in this article provides a closer prediction of the actual response. This is a clear indication that the use of heterogeneous fields instead of simplified homogeneous deformations increases the accuracy of the identification process.

It must be mentioned that this is the first attempt to apply an inverse method for material identification on plates under free air explosion. The first results look promising but there is still free space for improvements in different stages of the identification. In the present article the yield surface is assumed to be described by the von Mises yield criterion in order to limit the identification on the strain hardening parameter. However, the aluminum plates are fabricated through a rolling process and therefore, the effect of plastic anisotropy should be taken into account. Thus, the intention of the authors is to use an anisotropic yield criterion whose constants will be added as extra unknowns to the set of the parameters that the identification process aims to identify. In this work isotropic hardening is considered, while different types of hardening (kinematic or mixed isotropic kinematic) should be included in order to investigate the effect of the different types on the accuracy of the predicted response.

Acknowledgement

The authors would like to acknowledge the financial support from the Research Foundation Flanders (FWO) and the Flemish Agency for Innovation by Science and Technology (IWT).

References

Abda, A.B., Ameur, H.B., Jaoua, M., 1999. Identification of 2D cracks by boundary elastic measurements. Inverse Problems 15, 67–77.

Andrieux, S., Abda, A.B., Bui, H.D., 1997. Sur l'identification de fissures planes via le concept d'écart à la réciprocité. Comptes Rendus de l'Académie des Sciences Série II (324), 1431–1438.

Ardito, R., Bartalotta, P., Ceriani, L., Maier, G. 2003. Diagnostic inverse analysis of concrete dams with statical excitation. In Proceedings of the 5th Euromech Solid Mechanics Conference ESMC, Thessaloniki, Greece.

Avril, S., Bonnet, M., Bretelle, A.S., Grèdiac, M., Hild, F., Ienny, P., Latourte, F., Lemosse, D., Pagano, S., Pagnacco, E., Pieron, F., 2008. Overview of identification methods of mechanical parameters based on full-field measurements. Experimental Mechanics 48, 381–402.

Avril, S., Pierron, F., Sutton, M., Yan, J., 2008. Identification of elasto-viscoplastic parameters and characterization of Lüders behavior using digital image correlation and the virtual fields method. Mechanics of Materials 40, 729–742.

Avril, S., Pierron, F., Pannier, Y., Rotinat, R., 2008. Stress reconstruction and constitutive parameter identification in plane-stress elasto-plastic problems using surface measurements of deformation fields. Experimental Mechanics 48, 403–420.

Baker, W.E., Cox, P.A., Westine, P.S., Kulesz, J.J., Strehlow, R.A., 1983. Explosion Hazards and Evaluation. Elsevier Scientific Publishing Company, USA.

Becker, T., Splitthof, K., Siebert, T., Kletting, P. 2006. Error estimations of 3D digital image correlation measurements. In: Proceedings of The International Conference Speckle06: Speckles, From Grains to Flowers, Nimes, France.

Børvik, T., Hanssen, A.G., Langseth, M., Olovsson, l., 2009. Response of structures to planar blast loads – a finite element engineering approach. Computers and Structures 87, 507–520.

Bui, H.D. 1995. Sur quelques problèmes inverses élastiques en mècanique de l'endommagement. Deuxième colloque national de calcul de structures, Hermès, Lyon, pp. 26–35.

Bui, H.D., Constantinescu, A., Maigre, H., 2004. Numerical identification of linear cracks in 2D elastodynamics using the instantaneous reciprocity gap. Inverse Problems 20, 993–1001.

Calderon, A.P. 1980. On an inverse boundary value problem. In: Seminar on numerical analysis and its applications to continuum physics, Sociedade Brasileira de Matemática, Rio de Janeiro, pp. 65–73.

Chalal, H., Avril, S., Pierron, F., Meraghni, F., 2006. Experimental identification of a damage model for composites using the grid technique coupled to the virtual fields method. Composites Part A 37 (2), 315–325.

Christoulis, D.K., Guetta, S., Guipont, V., Jeandin, M., 2011. The influence of the substrate on the deposition of cold-sprayed titanium: an experimental and numerical study. Journal of Thermal Spray Technology 20 (3), 523–533.

Chu, T., Ranson, W., Sutton, M., Peters, W., 1985. Applications of digital image correlation techniques to experimental mechanics. Experimental Mechanics 25, 232–244.

Constantinescu, A., 1995. On the identification of elastic moduli from displacement-force boundary measurements. Inverse Problems in Engineering 1, 293–315.

Cooreman, S., Lecompte, D., Sol, H., Vantomme, J., Debruyne, D., 2007. Elasto-plastic material parameter identification by inverse methods: calculation of the sensitivity matrix. International Journal of Solids and Structures 44 (13), 4329–4341.

Cooreman, S., Lecompte, D., Sol, H., Vantomme, J., Debruyne, D., 2008. Identification of mechanical material behavior through inverse modeling and DIC. Experimental Mechanics 48, 421–433.

Coppieters, S., Cooreman, S., Sol, H., Van Houtte, P., Debruyne, D., 2011. Identification of the post-necking hardening behaviour of sheet metal by comparison of the internal and external work in the necking zone. Journal of Materials Processing Technology 211 (3), 545–552.

Cordero, R., Labbé, F., 2005. Uncertainty evaluation of displacement gradients measured by electronic speckle pattern shearing interferometry (ESPSI). Measurement Science and Technology 16, 1677–1683.

Cordero, R., Martinez, A., Rodriguez-Vera, R., Roth, P., 2004. Uncertainty evaluation of displacements measured by electronic speckle-pattern interferometry. Optics Communications 241, 279–292.

Cowper, G., Symonds, P.S. 1957. Strain-hardening and strain-rate effects in the impact loading of cantilever beams. Brown University Department of Applied Mathematics, Technical Report 28, USA.

Fundamentals of Protective Design for Conventional Weapons. 1986, U.S. Department of the Army (DATM), USA.

De Visscher, J. 1995. Identification of the complex stiffness matrix of orthotropic materials by a mixed numerical experimental method. PhD Thesis, Vrije Universiteit Brussel, Brussels, Belgium.

Ferin, G., Certon, D., Guyonvarch, J., Felix, N. 2004. Inverse calculation method for piezocomposite materials characterization. In: proceedings of IEEE International Ultrasonics, Ferroelectrics, and Frequency Control Conference, Montreal, Canada.

Flores, P., Duchene, L., Bouffioux, C., Lelotte, T., Henrard, C., Pernin, N., Van Bael, A., He, S., Duflou, J., Habraken, A.M., 2007. Model identification and FE simulations: effect of different yield loci and hardening laws in sheet forming. International Journal of Plasticity 23 (3), 420–449.

Förster, F., 1937. Ein neues Messverfahren zur Bestimmung des Elastizitats moduls und der Dampfungrster (1937).. Zeitshrift für Metalkunde 29, 109–115.

Furukwaw, T., Yagawa, G., 1998. Implicit constitutive modelling for viscoplasticity using neural networks. International Journal for Numerical Methods in Engineering 43, 195–219.

Genovese, K., Lamberti, L., Pappalettere, C., 2006. Mechanical characterization of hyperelastic materials with fringe projection and optimization techniques. Optics and Lasers in Engineering 44, 423–442.

Geymonat, G., Pagano, S., 2003. Identification of mechanical properties by displacement field measurement: a variational approach. Meccanica 38, 535–545.

Geymonat, G., Hild, F., Pagano, S., 2002. Identification of elastic parameters by displacement field measurement. Comptes Rendus Mécanique 330, 403–408.

Ghouati O., Gelin, J. 1998. Identification of material parameters directly from metal forming processes. Journal of Materials Processing Technology 80–81, pp. 560–564.

Grédiac, M., Pierron, F., 2006. Applying the Virtual Fields Method to the identification of elasto-plastic constitutive parameters. International Journal of Plasticity 22 (4), 602–627.

Hadj-Sassi, K., Andrieux, S. 2007. Une nouvelle fonctionnelle d'énergie incrmentale totale pour le controle des parties rversibles et dissipatives des matriaux standards. In: Actes du Huitième Colloque National en Calcul des Structures, Hermes, Lyon, pp. 255–261.

Hendriks, F., Brokken, D., van Eemeren, J., Oomens, C., Baaijens, F., Horsten, J., 2003. A numerical–experimental method to characterize the nonlinear mechanical behaviour of human skin. Skin Research and Technology 9, 274–283.

Hikawa, A., Kawahara, M., Kaneko, N. 2004. Parameter identification of ground elastic modulus at tunnel excavation site. Annual report of the Kawahara Laboratory, Chuo University, Japan.

Hoes, K., Dinescu, D., Sol, H., Parnas, R., Lomov, S., 2004. Study of nesting induced scatter of permeability values in layered reinforcement fabrics. Composites Part A 35, 1407–1418.

Ikehata, M., 1990. Inversion formulas for the linearized problem for an inverse boundary value problem in elastic prospection. SIAM Journal on Applied Mathematics 50 (6), 1635–1644.

Jadhav, A., Farmani, R., Toropov, V., Snee, M., 1999. Identification of parameters for air permeability of shotcrete tunnel lining using a genetic algorithm. Computers and Geotechnics 25, 1–24.

Johnson, G.R., Cook, W.H. 1983. A constitutive model and data for metals subjected to large strains, high strain rates and high temperatures. In: proceedings of the Seventh International Ballistics Symposium, The Hague, pp. 541–548.

Jones, N., 1989. Structural Impact. Cambridge University Press, UK.

Kauer, M. 2006. Inverse finite element characterization of soft tissues with aspiration experiments. PhD Thesis, Swiss Federal Institute of Technology, Zurich, Switzerland.

Kavanagh, K.T., Clough, R.W., 1971. Finite element applications in the characterization of elastic solids. International Journal of Solids and Structures 7, 11–23.

Kingery, C.N., Bulmash, G. 1984. Air blast parameters from TNT spherical air burst and hemispherical surface burst, U.S. Army Ballistic Research Laboratory USA.

Latourte, F., Chrysochoos, A., Pagano, S., Wattrisse, B., 2008. Elasto-plastic behavior identification for heterogeneous loadings and materials. Experimental Mechanics 48, 435–449.

Lecompte, D. 2007. Elastic and elasto-plastic material parameter identification by inverse modeling of static tests using digital image correlation. PhD thesis: Vrije Universiteit Brussel and Koninklijke Militaire School, Brussels, Belgium.

Lecompte, D., Sol, H., Vantomme, J., Habraken, A.M. 2005. Identification of elasto-plastic orthotropic material parameters based on ESPI measurements. In: Proceedings of SEM Annual Conference Portland, USA, pp. 7–9.

Lecompte, D., Smits, A., Sol, H., Vantomme, J., Van Hemerlrijck, D., 2007. Mixed numerical experimental technique for orthotropic parameter identification using biaxial tensile tests on cruciform specimens. International Journal of Solids and Structures 44, 1643–1656.

Levenberg, K., 1944. A method for the solution of certain non-linear problems in least squares. Quarterly of Applied Mathematics 2, 164–168.

Livermore Software Technology Corporation (LSTC), 2007. LS-DYNA User's Manual: Nonlinear Dynamic Analysis of Structures (Version 971), USA.

Mahnken, R., Stein, E., 1996. A unified approach for parameter identification of inelastic material models in the frame of the finite element method. Computer Methods in Applied Mechanics and Engineering 136, 225–258.

Marquardt, D.W., 1963. An algorithm for least-squares estimation of nonlinear parameters. SIAM Journal on Applied Mathematics 11 (2), 431–441.

Mauvoisin, G., Bremand, F.J., Lagarde, A., 1994. Three-dimensional shape reconstruction by phase-shifting shadow moire. Applied Optics 33, 2163–2169.

Meuwissen, M., 1998. An inverse method for the mechanical characterization of metals. PhD Thesis, Eindhoven University of Technology, Eindhoven, The Netherlands.

Molimard, J., Le Riche, R., Vautrin, A., Lee, J.R., 2005. Identification of the four orthotropic plate stiffnesses using a single open-hole tensile test. Experimental Mechanics 45 (5), 404–411.

Moreau, A., Pagnacco, E., Borza, D., Lemosse, D. 2006. An evaluation of different mixed experimental/numerical procedures using FRF for the identification of viscoelastic materials. In: Proceedings of ISMA Conference Leuven, Belgium, pp. 18–20.

Nguyen, H.M., Allix, O., Feissel, P. 2006. Application of the CRE for parameter identification in nonlinear dynamics with corrupted measurements. In: Seventh World Congress on Computational Mechanics Los Angeles, USA.

Nicoletto, G., 2002. On the visualization of heterogeneous plastic strains by Moire interferometry. Optics and Lasers in Engineering 37, 433–442.
Pagnacco, E., Moreau, A., Lemosse, D., 2007. Inverse strategies for the identification of elastic and viscoelastic material parameters using full-field measurements. Materials Science Engineering A 452, 737–745.
Panneton, R., Atalla, Y., Blanchet, D., Bloor, M. 2003. Validation of the inverse method of acoustic material characterization. In: Proceedings of the 2003 SAE Noise & Vibration conference, Traverse City, Michigan, USA.
Qu, J., Jin, Q.L., Xu, B.Y., 2005. Parameter identification for improved viscoplastic model considering dynamic recrystallization. International Journal of Plasticity 21 (7), 1267–1302.
Randers-Pehrson, G., Bannister, K.A. 1997. Airblast Loading Model for DYNA2D and DYNA3D. Report ARBL-TR-1310, U.S. Army Ballistic Research Laboratory, USA.
Remennikov, A.M., 2003. A review of methods for predicting bomb blast effects on buildings. Journal of Battlefield Technology 6 (3), 5–10.
Schiltges, G. 1999. Continuum mechanical investigations on microstructures. PhD Thesis, Swiss Federal Institute of Technology, Zurich, Switzerland.
Schreier, H.W., Braasch, J.R., Sutton, M.A., 2006. Systematic errors in digital image correlation caused by intensity interpolation. Optical Engineering 39 (11), 2915–2921.
Smith, P.D., Hetherington, J.G., 1994. Blast and Ballistic Loading of Structures. Butterworth-Hineman, UK.
Spranghers, K., Vasilakos, I., Lecompte, D., Sol, H., Vantomme, J., 2012. Full-field deformation measurements of aluminum plates under free air blast loading. Experimental Mechanics 52, 1371–1384. http://dx.doi.org/10.1007/s11340-012-9593-5.
Spranghers, K., Vasilakos, I., Lecompte, D., Sol, H., Vantomme, J., 2012. Numerical simulation and experimental validation of the dynamic response of aluminum plates under free air explosions. International Journal of Impact Engineering 54, 83–95. http://dx.doi.org/10.1016/j.ijimpeng.2012.10.014.
Sutton, M.A., Orteu, J., Schreier, H.W., 2009. Image Correlation for Shape Motion and Deformation Measurements. Springer, USA.
Tarantola, A., 2004. Inverse Problem Theory and Methods for Model Parameter Estimation. SIAM, Paris, France.
Tiwari, V., Sutton, M.A., McNeill, S.R., 2007. Assessment of high speed imaging systems for 2D and 3D deformation measurements: methodology development and validation. Experimental Mechanics 47, 561–579.
Trujillo, D., Busby, H., 1997. Practical Inverse Analysis in Engineering,, CRC Press, Boca Raton, Florida, USA, ISBN 0-8493965-9-X.
Yoshida, F., Urabe, M., Hino, R., Toropov, V., 2003. Inverse approach to identification of material parameters of cyclic elasto-plasticity for component layers of a bimetallic sheet. International Journal of Plasticity 19, 2149–2170.